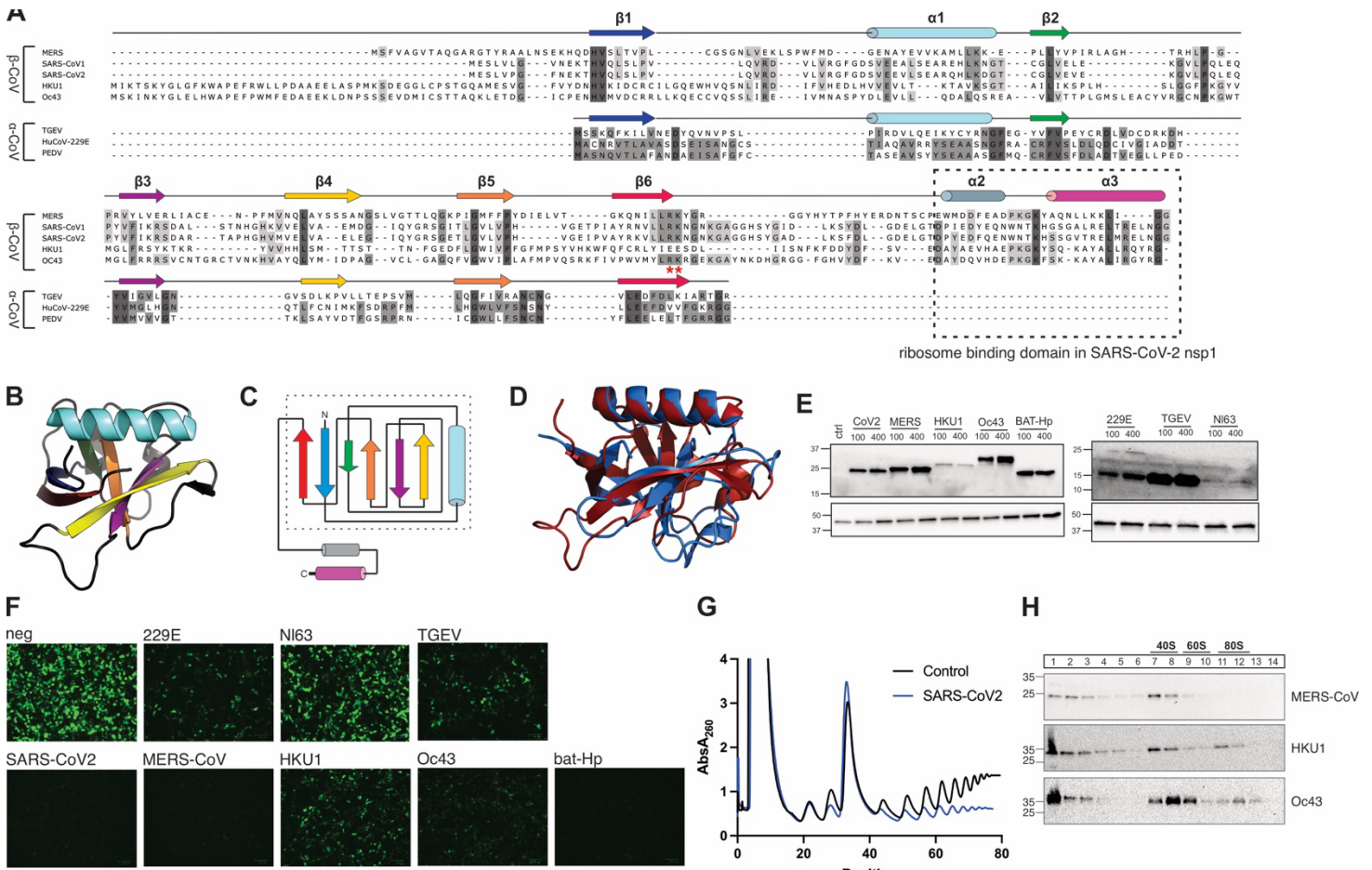# Supplementary Material

Figure S1: Sequence diversity but structural and functional conservation of Nsp1 from α- and β-coronaviruses. A) Sequence alignment of Nsp1 from various α- and β-coronaviruses. Multiple sequence alignments of α-CoV Nsp1 and β-CoV Nsp1 sequences were performed independently, and manually aligned based on structure conservation. B) N-terminal globular domain of SARS-CoV-2 (pdb: 7k7p) C) Schematic representation of the SARS-CoV-2 fold, secondary structure elements are colored to match B. Box depicts NTD D) Overlay of the NTD of SARS-CoV-2 Nsp1 (in red, pdb 7k7p) and full-length TGEV Nsp1 (in blue, pdb: 6IVC). Note the similarity in 3D structure despite considerable sequence variation. E) α-FLAG immunoblot analysis 3x-FLAG Nsp1 proteins from the indicated viruses and ACTB as a loading control. F) Host shutoff in HEK293T cells transiently expressing Nsp1 from the indicated viruses and EGFP reporter gene. G) Sucrose gradient profile of cells transiently overexpressing 3xFLAG-Nsp1(SARS-CoV-2) or an empty vector control. H) Anti-FLAG immunoblot of fractions 1-14 from sucrose gradient analysis of HEK293T cells transiently overexpressing 3xFLAG-Nsp1 from MERS-CoV, HuCoV-HKU1 or HuCoV-OC43. Fractions containing 40S, 60S and 80S ribosomal subunits are indicated on the top.
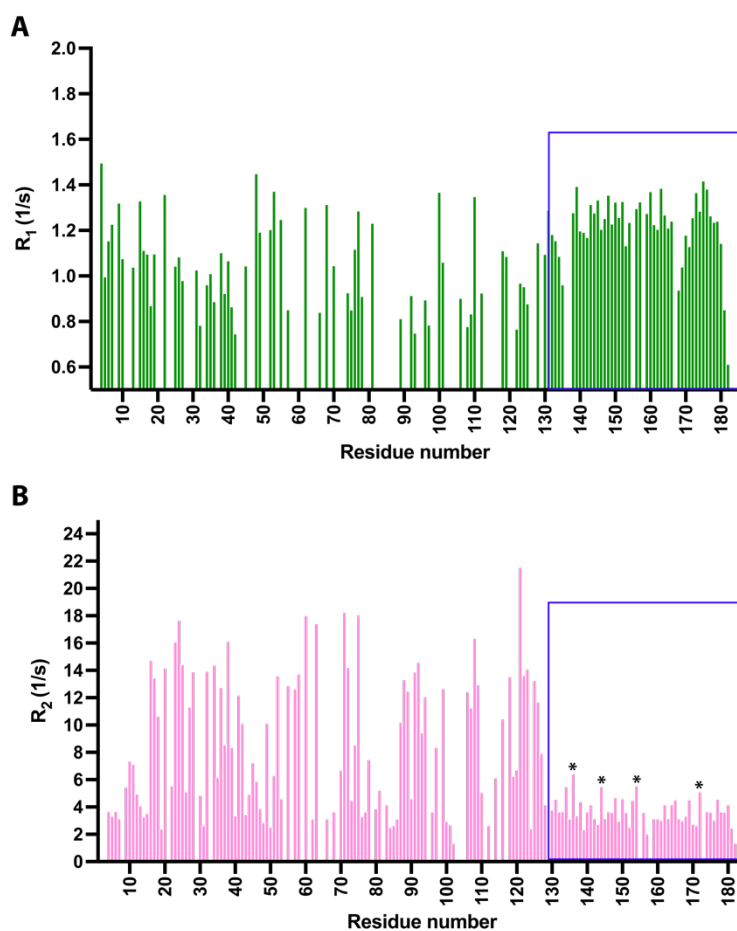
Figure S2: NMR relaxation experiments show the intrinsically disordered CTD of Nsp1. A) ^{15}N longitudinal relaxation rates R_1. B) ^{15}N transverse relaxation rates R_2. Analysis of R_2 relaxation data showed an average R_2 value of 6.8 s^{-1} and a decrease in relaxation rates from residues G-127. Measurements were conducted at 600 MHz field strength. The purple box marks the CTD. The asterisks denote CTD residues His-134, Ser-141, Asp-152, Thr-170, that have higher than average R_2, demonstrating structural compaction and/or exchange on the µs-ms timescale.
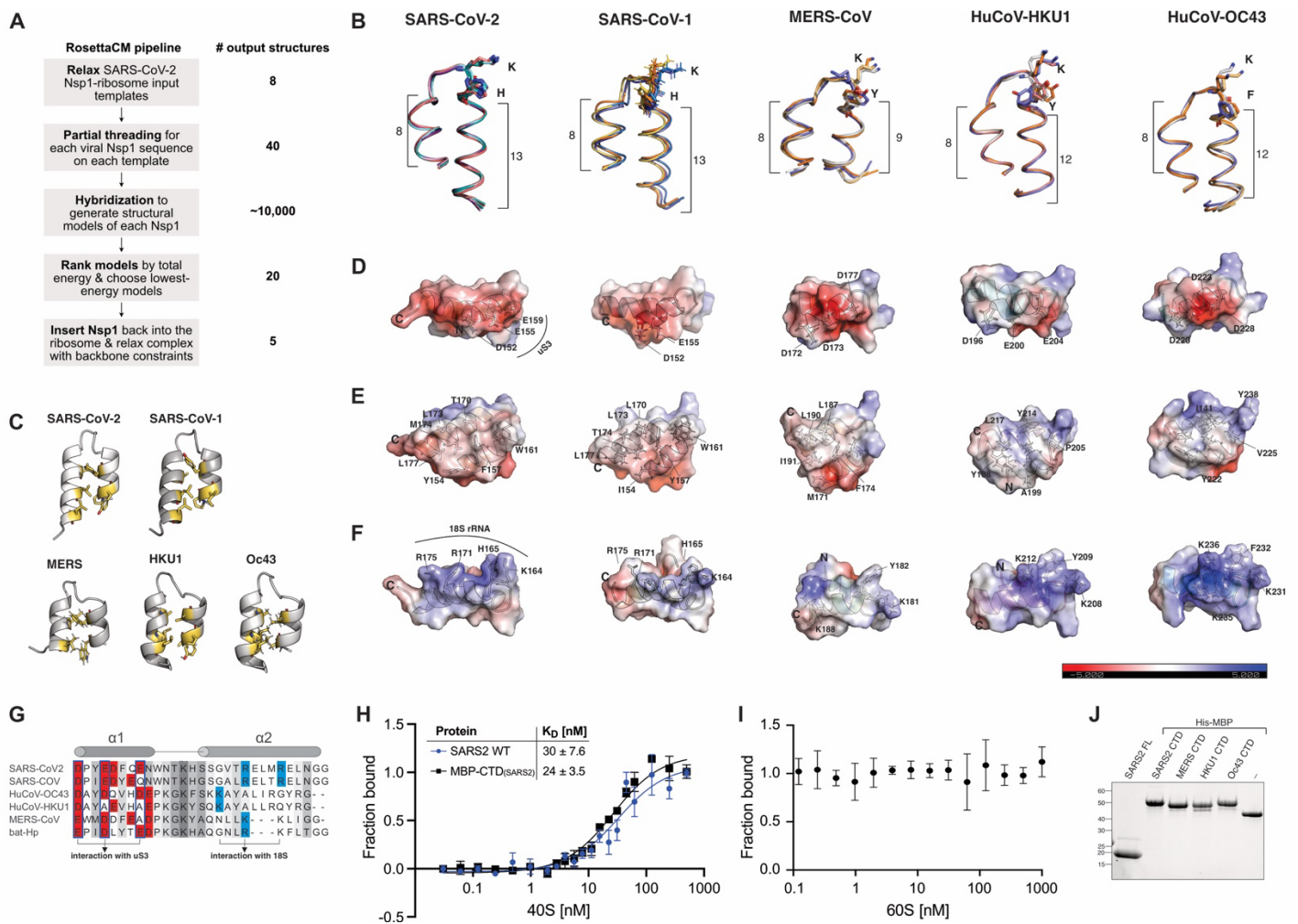
Figure S3: Modeling of the C-terminal domain from diverse β-CoV Nsp1. A) Overview of the homology modeling pipeline. B) Overlay of the Rosetta models of the Nsp1 CTD from the indicated β-CoVs. The conserved KH or KY/F motif is shown in the loop. Numbers indicate the length (in amino acids) of α-helix 1 and 2. C) Hydrophobic residues at the helix interface stabilize the Nsp1 CTD. D-F) Electrostatic surface representation of the Nsp1 CTD models shows partial surface charge conservation between divers Nsp1 variants. Electrostatics were calculated using the Adaptive Poisson-Boltzmann Solver (APBS) in pymol. The surface colors are fixed at red (-5) and blue (+5). G) Sequence alignment of the Nsp1 CTD from SARS-CoV, SARS-CoV-2, MERS-CoV, HuCoV-HKU1, HuCoV-OC43 and bat-Hp nsp1. Negatively charged amino acids in helix 1 are depicted in red, and positively charged amino acids in helix 2 are depicted in blue. Note that the charged amino acids are positioned differently along the helices. H) Equilibrium binding measurements of FAM-labeled SARS-CoV-2 Nsp1 and MBP-CTD$_{SARS2}$ to purified rabbit 40S ribosomal subunits in buffer containing 250 mM K$^+$. n=3, error bars=SEM. I) 60S ribosomal subunits do not compete with Nsp1 for 40S ribosomal subunit binding. 5 nM FAM-labeled SARS-CoV-2 Nsp1 was pre-incubated in the presence of 100 nM 40S ribosomal

subunits, and equilibrium binding measurements performed in the presence of the indicated concentrations of 60S ribosomal subunits. All experiments were performed in buffer containing 125 mM K$^+$. n=4, error bars = SD. J) Purified recombinant proteins used in this study.
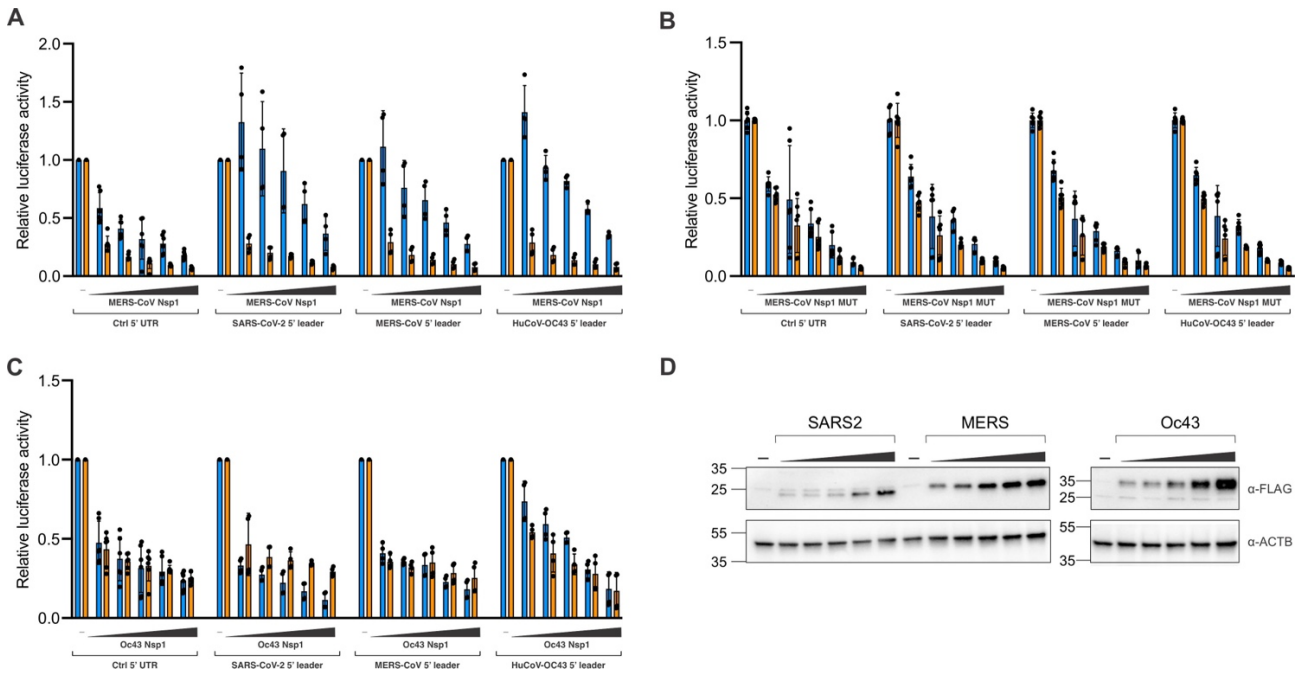
Figure S4: No virus-specific RNA-protein interactions modulate MERS-CoV and HuCoV-OC43 Nsp1 function. A-C) Nsp1-dependent host shutoff and translation boost in HEK293T cells transiently expressing MERS-CoV Nsp1 (A), MERS-CoV Nsp1 (RK-146/7-AA) (B), or HuCoV-OC43 Nsp1 (C) and FLuc reporters with the indicated 5' UTRs. NLuc was co-transfected as an internal control. N=6, error bars = SD. D) Representative immunoblot analysis showing the expression levels of Nsp1.